A Comparison of Global Lithospheric Field Models Derived from Satellite Magnetic Data

Kumar Hemant and Stefan Maus

GeoForschungsZentrum, Division 2.3, Telegrafenberg, D-14473 Potsdam

Summary. Satellite missions over more than three decades, have added immensely to our understanding of the geomagnetic field. Here, we give a comparison of the lithospheric field models, prepared by various workers from POGO, Magsat, Ørsted and CHAMP satellite data. Mapping the global lithospheric anomalies requires careful reductions which include the main field, its secular variation (SV) and corrections for the external magnetospheric and ionospheric contributions to the data recorded by satellite. The discrepancies between the various maps are mainly due to differences in the rigor with which the data is processed, in the selection of the magnetically quiet periods and in the algorithms used to estimate the spherical harmonic coefficients of scalar potential or the total intensity of the field. The models also strongly differ in how the magnetospheric and ionospheric contributions have been detected and eliminated in order to correct the equatorial, mid-latitude and polar latitude data. We plot the anomaly of the total intensity of the field at 450 km altitude (except ALP94 which is at 400 km).

Key words: Power spectra, filtering, lithospheric, field models

1 Introduction

The POGO (1965-1971) satellite missions, Magsat (1979-1980) and more recently Ørsted (February 1999 onward), CHAMP (July 2000 onward) and SAC-C (November 2001 onward) in near-Earth orbits have helped us to understand not only the Earth's main field but also the external fields with sources in the ionosphere and magnetosphere. Based on the available satellite and observatory data, several lithospheric anomaly maps have been prepared over the last two decades. One way to visualize the developments and evolution of different lithospheric field models is to compare their power spectra. Figure 1 shows the power spectra (Arkani-Hamed et al., 1994) of the total intensity anomaly at 450 km altitude of several lithospheric field models together with the spectrum of our CHAMP map. The comparison of power spectra of different lithospheric field models shows a discrepancy by an order of magnitude. As discussed below, these models can be categorized in two classes according to the different processing techniques employed to arrive at the final anomaly maps. The first set of global maps employ various filtering techniques to arrive at the anomaly map, while the second set does not apply any filters.

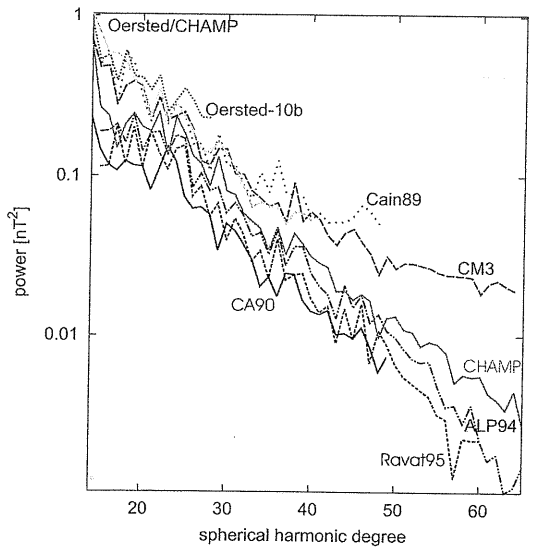

Fig. 1. Power Spectra of the total intensity anomaly (Arkani-Hamed et al., 1994) at 450 km altitude of several Magsat and POGO, Ørsted and CHAMP lithospheric field models

2 Class I: Models based on along-track filtered data

Cohen and Achache (1990) derive the potential of the lithospheric field using Magsat data up to spherical harmonic degree and order 14-50 as shown in Fig. 2. Instead of the index K_p, a 3 hour global index A_m, based on 24 observatories is used. To obtain the residual field, a main field model is subtracted from the measured field and then each component is averaged over 1-s interval to reduce high-frequency noise and the effect of external magnetic disturbances. A mean equatorial anomaly (MEA) is computed by averaging all corrected profiles plotted at constant dip latitude to correct for equatorial electrojects(EEJs). North-south filtering is done on the data set. After the least squares inversion of the spherical harmonic coefficients of the potential, the resulting discrepancies between dawn and dusk averages are less than 1 nT.

Arkani-Hamed et al (1994) present a scalar magnetic anomaly map(ALP94) from combined data sets of the POGO and Magsat satellites. Magsat scalar anomaly map used here was derived by Ravat et al. (1995) using Magsat dawn and dusk and POGO scalar anomaly map at an altitude of 400 km using POGO data. Two anomaly maps are derived based on two selection criteria: stringent and less-string ent. The stringent criteria seek to isolate anomaly signal of lithospheric origin by eliminating signals of remaining unmodeled main field, its secular variation and of external origin (ring currents), but at the expense of suppressing some

lithospheric anomaly signal. The map shown in Fig. 3 is represented by spherical harmonic of degree 15-60. The map based on less-stringent criteria seeks to encompass maximum signals of lithospheric origin. The map is not shown here. Accuracy for the maps is estimated by the authors to be ± 2 nT.

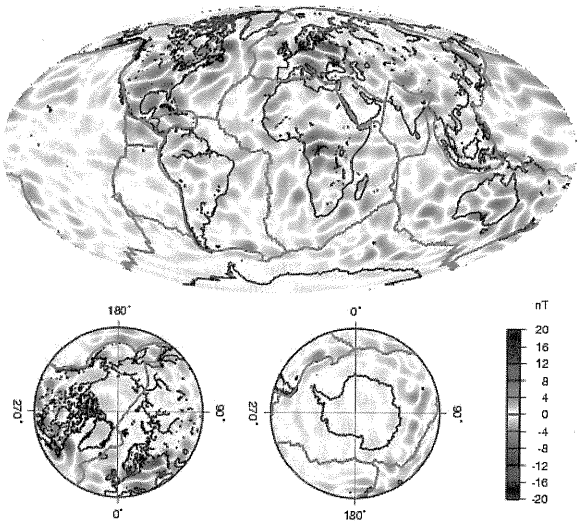

Fig. 2. Global scalar anomaly map prepared using Magsat vector data (Cohen and Achache, 1990)

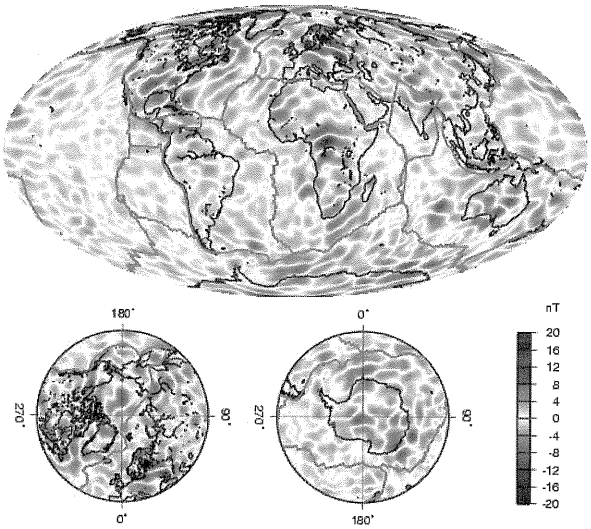

Fig. 3. Global scalar anomaly map prepared using Magsat dusk and dawn data and POGO satellite data (Arkani-Hamed et al, 1994)

Ravat et al (1995) Scalar anomaly map shown in Fig. 4 is derived using scalar Magsat dawn and dusk data for spherical harmonic degrees 15-65. The data selection for magnetic quiet days uses index K_p less than 2^+ for equatorial and mid-latitudes and AE index less than 50 nT for polar latitudes while the variance for the residual (ΔB) is kept at less than 80 $(nT)^2$. High pass Kaiser filter with a cut-off wavelength of 4000 km is applied, to remove the magnetic fields due to ionospheric current systems. To remove the inconsistencies between the near-by passes and between dawn and dusk data, pass-by-pass correlation followed by crossover analysis is carried out. Equivalent source dipole representations are used to generate the scalar anomaly map. Covariant spherical harmonic analysis is used to isolate the 'common features' of dawn and dusk data.

Maus et al (2002) The CHAMP satellite data were processed in 120^0 track segments at the mid-equatorial latitudes and 100^0 track segments at the poles. Mid-latitude data is selected between 22:00 – 6:00 LT. A planetary activity index K_p less than 2^+ is used for the selection of magnetically quiet days. After subtracting a recent Ørsted main and external field model, the remaining unmodeled large-scale external contribution is removed by fitting a homogeneous field and subtracting it on a track by track basis. In order to preserve N/S trending features, the data are not filtered further along-track. At the poles, a subset of quiet data with minimum root mean square (rms) is chosen for the analysis. Spherical harmonic coefficients 15-65 of the magnetic potential are estimated by a least squares minimum norm procedure. The anomaly map is shown in Fig. 5.

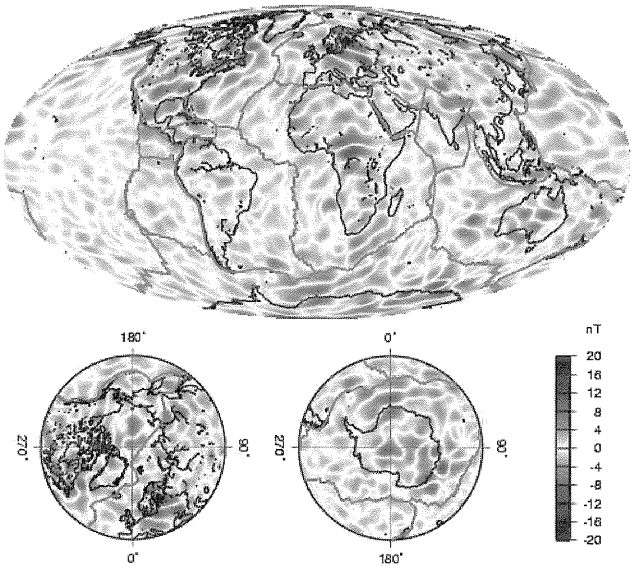

Fig. 4. Global scalar anomaly map prepared using Magsat scalar data (Ravat et al, 1995)

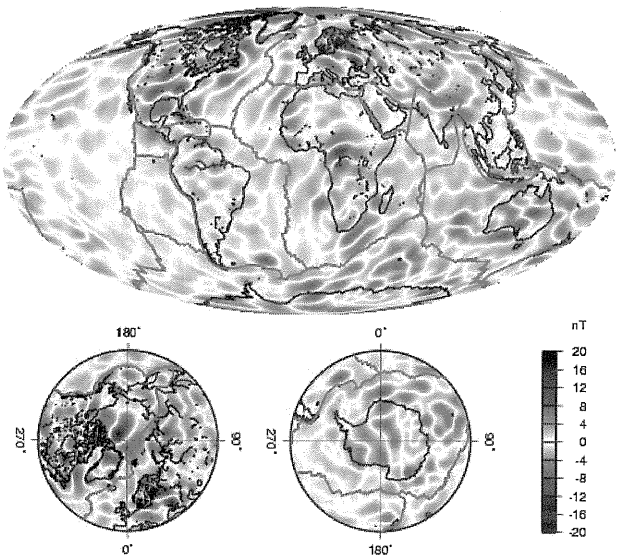

g. 5. Global scalar anomaly map prepared using CHAMP scalar data (Maus et al, 2002)

Class II: No filtering

ıe following set of scalar anomaly maps applies no filtering techniques to arrive their final models.

ain et al (1989a) Scalar magnetic anomaly map shown in Fig. 6 is derived for herical harmonic degrees 14-63. A selection of observed Magsat vector data is ken and averaged over data blocks of 3^0 x 3^0 in size. Data are selected for inter- ls with K_p less than 2^+. After D_{st} correction, residuals are corrected for iono- heric currents. The spherical harmonic coefficients are derived up to n=63, wever the spectrum computed by Cain et al (1989b) is claimed to be correct up n=59, beyond which it is said to be plagued with noise. The average altitude of e anomaly map is 450 km., however no altitude correction to the data has been rformed and this can be a source of error.

M3 **Model (2000)** A new model as shown in Fig. 7, called CM3 (Compre- hen- ve Model: Phase 3) has been derived using the Magsat and Pogo satellite data d incorporating observatory hourly and annual means data. The spherical har- onic expansion is done to degree/order 14-65 in order to account for fields from e Earth's lithosphere at satellite altitude. Data selection procedure considers the dex K_p less than 1^- and the Magsat dawn and dusk data are selected with $|D_{st}|$ s than 20 nT. Special quasi-dipole (QD) conforming harmonic functions have

been used, including terms accounting for seasonal variation and variation with solar activity. Least squares inversion is performed to arrive at the comprehensive model. The fit to the data is much better than in its predecessor models.

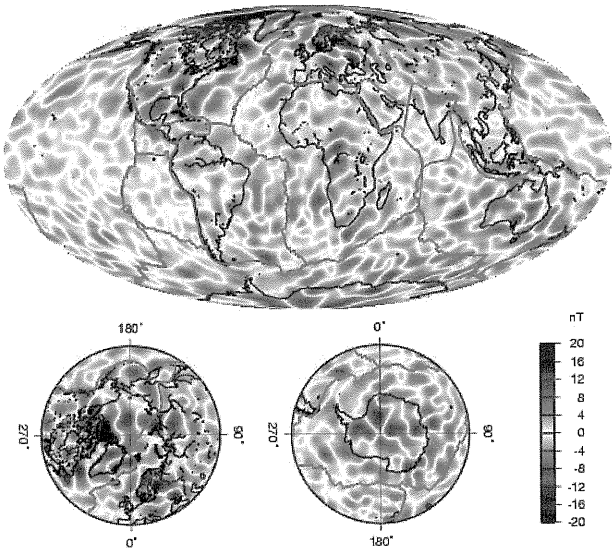

Fig. 6. Global scalar anomaly map prepared using Magsat vector data (Cain et al, 1989a)

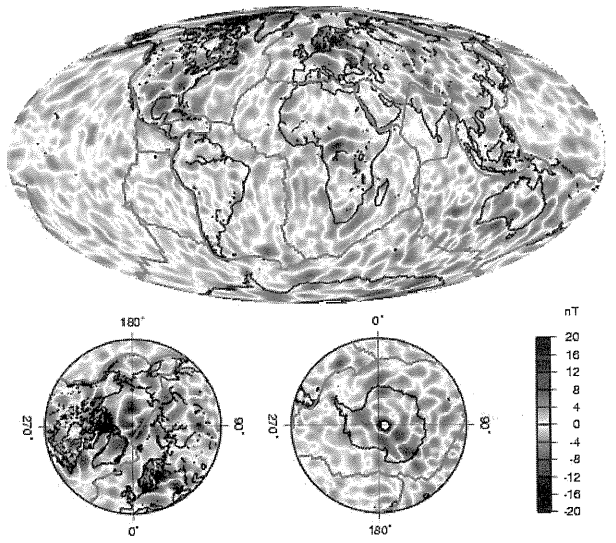

Fig. 7. Global scalar anomaly map prepared using Magsat vector and Pogo scalar data (Sabaka et al, 2000).

Olsen (2001) A spherical harmonic model, Ørsted_01c_o2, of the lithospheric field up to degree 41 and of the secular variation up to degree 13 is derived using Ørsted satellite data as shown in Fig. 8. The quiet data selection is based on index K_p equal to 1^+. At the polar caps data recorded with IMF (Inter-planetary magnetic fields) field $|B_y|$ greater than 3 nT is rejected. A modified D_{st} index derived from data of ground-based observations was used. Magnetospheric contributions are modeled up to degree/order 2 with zonal terms varying with annual and semi-annual periodicity. The model is estimated using Iteratively Re-weighted Least Squares with Huber weights to account for the non-Gaussian data error distribution. RMS misfit to the data is 3 nT. The model predicts scalar observations from CHAMP satellite very well with an rms misfit of 3.5nT at non-polar latitudes and about 6 nT at polar latitudes.

Over the coming years, a continuous stream of high quality magnetic data from several near Earth satellites will allow increasingly accurate simultaneous modeling of the main, lithospheric and ionospheric fields. These modeling results will help us remove the effects of the external sources and the main field contribution to the internal field to produce a more accurate global lithospheric field model. The new field models will thus provide a new basis for the study of crustal composition, dynamics and heat flow.

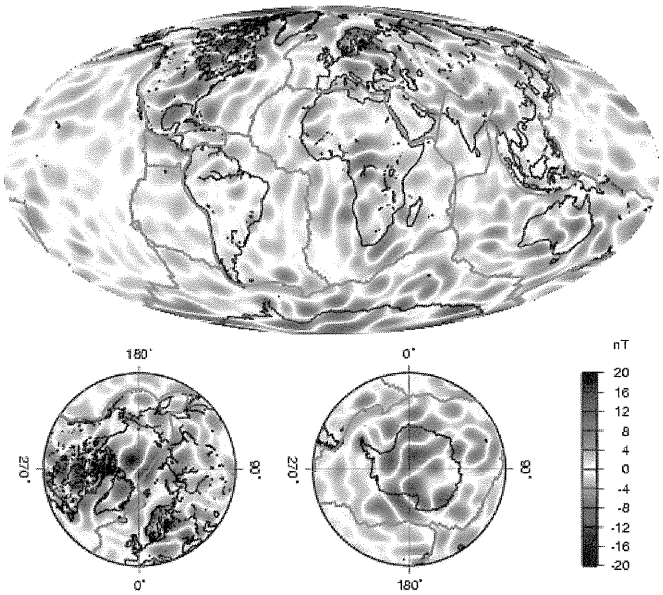

Fig. 8. Global scalar anomaly map prepared using CHAMP and Ørsted vector data (Olsen, 2001).

References

Arkani-Hamed J, Langel RA, Purucker ME (1994) Magnetic anomaly maps of Earth derived from POGO and Magsat data. J Geophys Res 99: 24075-24090.

Cain JC, Schmitz DR, Muth L (1984) Small-scale features in the earth's magnetic field observed by Magsat. J Geophys Res 89: 1070-1076.

Cain JC, Wang Z, Kluth C, Schmitz DR (1989a) Derivation of a geomagnetic model to n = 63. Geophys J 97: 431-441.

Cain JC, Wang Z, Schmitz DR, Meyer J (1989b) The geomagnetic spectrum for 1980 and core-crustal separation. Geophys J 97: 443-447.

Cohen Y, and Achache J (1990) New global vector anomaly maps derived from Magsat data. J Geophys Res 95: 10783-10800.

Langel RA (1990) Global magnetic anomaly maps derived from POGO spacecraft data. Phys. Earth Planet. Inter. 62: 208-230.

Maus S, Rother M, Holme R, Luhr H, Olsen N, Haak V (2002) First CHAMP satellite magnetic data resolve uncertainty about strength of the lithospheric magnetic field. Geophys Res Letts (in press)

Olsen N (2001) A model of the Geomagnetic Main Field and its Secular Variation for Epoch 2000 Estimated from Ørsted Data. Geophys J Int(in press)

Ravat D, Langel RA, Purucker M, Arkani-Hamed J, Alsdorf DE (1995) Global vector and scalar Magsat magnetic anomaly maps. J Geophys Res 100: 20111-20136.

Sabaka TJ, Olsen N, Langel RA (2000) A comprehensive model of the near-Earth Magnetic Field: Phase 3. NASA/TM-2000-209894, National Aeronautics and Space Administration, Goddard Space Flight Center, Greenbelt, Maryland.

Schmitz DR, Meyer J, Cain JC (1989) Modelling the Earth's geomagnetic field to high degree and order. Geophys J R Astr Soc 97: 421-430.